AGU PUBLICATIONS

Geophysical Research Letters

RESEARCH LETTER
10.1002/2015GL064574

Key Points:
- First AMISR-14 observations
- Detection of submeter ESF irregularities
- Temporal and spatial variability of ESF

Correspondence to:
F. S. Rodrigues,
Fabiano@utdallas.edu

Citation:
Rodrigues, F. S., M. J. Nicolls, M. A. Milla, J. M. Smith, R. H. Varney, A. Strømme, C. Martinis, and J. F. Arratia (2015), AMISR-14: Observations of equatorial spread *F*, *Geophys. Res. Lett.*, *42*, 5100–5108, doi:10.1002/2015GL064574.

Received 22 MAY 2015
Accepted 7 JUN 2015
Accepted article online 11 JUN 2015
Published online 7 JUL 2015

AMISR-14: Observations of equatorial spread *F*

F. S. Rodrigues[1], M. J. Nicolls[2], M. A. Milla[3], J. M. Smith[1], R. H. Varney[2], A. Strømme[2], C. Martinis[4], and J. F. Arratia[5]

[1]William B. Hanson Center for Space Sciences, University of Texas at Dallas, Richardson, Texas, USA, [2]SRI International, Menlo Park, California, USA, [3]Jicamarca Radio Observatory, Lima, Peru, [4]Center for Space Physics, Boston University, Boston, Massachusetts, USA, [5]Student Research Development Center, Ana G. Mendez University System, San Juan, Puerto Rico

Abstract A new, 14-panel Advanced Modular Incoherent Scatter Radar (AMISR-14) system was recently deployed at the Jicamarca Radio Observatory. We present results of the first coherent backscatter radar observations of equatorial spread *F* (ESF) irregularities made with the system. Colocation with the 50 MHz Jicamarca Unattended Long-term studies of the Ionosphere and Atmosphere (JULIA) radar allowed unique simultaneous observations of meter and submeter irregularities. Observations from both systems produced similar Range-Time-Intensity maps during bottom-type and bottomside ESF events. We were also able to use the electronic beam steering capability of AMISR-14 to "image" scattering structures in the magnetic equatorial plane and track their appearance, evolution, and decay with a much larger field of view than previously possible at Jicamarca. The results suggest zonal variations in the instability conditions leading to irregularities and demonstrate the dynamic behavior of *F* region scattering structures as they evolve and drift across the radar beams.

1. Introduction

The Advanced Modular Incoherent Scatter Radar (AMISR) technology was developed for radio remote sensing of the Earth's upper atmosphere and ionosphere and studies of the space weather. SRI International led the collaborative effort in the development of AMISR, whose novel modular configuration was designed to allow relative ease of relocation for studying upper atmospheric activity around the globe. Remote operation and electronic beam steering allow researchers to operate and position the radar beam on pulse-to-pulse basis to accurately measure rapidly changing space weather events that cannot be resolved with conventional radar systems.

Modularity is one of the strengths of AMISR. The most basic element of an AMISR system is the Antenna Element Unit (AEU). Each AEU is formed by a cross-dipole antenna, circuitry for phase control on receive and transmit operations, a 500 W solid state RF power amplifier, a power supply unit, and digital control and communication electronics. An AMISR panel is formed by 32 AEUs. Each panel contains a Panel Control Unit (PCU), which controls and monitors the AEUs. The PCU contains a fully programmable Linux computer, which can be adjusted and upgraded to maximize the functionality of the array. Finally, 128 panels are organized, roughly, in a square configuration (about 30 m × 30 m), to form a standard AMISR face. In addition to a number of prototype systems, two full AMISR faces have been built, deployed, and are currently in operation. A third will be deployed in the near future. A full AMISR face has a peak power of ~2 MW allowing observations of incoherent scattering of radio waves by thermal plasma waves [e.g., *Dougherty and Farley*, 1960].

The first AMISR face was deployed in 2007 at the Poker Flat Research Range in Alaska. The Poker Flat incoherent scatter radar is used for upper atmospheric studies in the auroral region in conjunction with a series of ground-based instruments, sounding rockets, and satellites. Another NSF-funded AMISR face was deployed in Resolute Bay, Canada, in 2009 for studies of the upper atmosphere in the polar cap region. The panel was positioned as to point to the north well into the polar cap and is referred to as RISR-N. Finally, a third AMISR face, RISR-C, is also located in Resolute Bay but points southward. This system will provide better coverage of the polar cap and will be operational in the near future.

The use of a smaller number of panels (which results in reduced power and aperture) reduces sensitivity to incoherent scatter. It is possible, however, to use a small system to make coherent backscatter observations of nonthermal plasma waves (irregularities). In 2004/2005, a seven-panel AMISR prototype was temporarily

deployed at the Jicamarca Radio Observatory (JRO) for tests and observations of low-latitude ionospheric irregularities. Observations of equatorial electrojet were possible [*Vlasov et al.*, 2007; *Hysell et al.*, 2007; *Kelley et al.*, 2008; *Kagan et al.*, 2008], but the system was not sensitive enough for adequate measurements of equatorial spread *F* (ESF).

Anticipating the deployment of an AMISR system in Argentina for conjugate studies with the Arecibo Observatory ISR, a 14-panel AMISR system (AMISR-14) was deployed to JRO with first light in August 2014. During the period between 14 and 28 August, a number of experiments were performed to test the system and study different types of field-aligned ionospheric irregularities, including those associated with the equatorial electrojet, 150 km echoes, and equatorial spread *F*.

Here we report the results of successful AMISR-14 observations of submeter scale size ionospheric irregularities associated with ESF events. ESF is the name given to a broad spectrum of electron density irregularities commonly observed in the equatorial and low-latitude *F* region ionosphere during postsunset hours [e.g., *Woodman*, 2009]. ESF has been observed using vertical radio sounders, optical instrumentation, and sensors for in situ measurements onboard rockets and satellites [e.g., *McClure et al.*, 1977; *Abdu et al.*, 1983; *LaBelle et al.*, 1997; *Makela and Miller*, 2008]. It has also been studied using a number of numerical models [e.g., *Huang et al.*, 1993; *Huba et al.*, 2010; *Retterer*, 2010; *Aveiro and Hysell*, 2010]. It has been found that ESF occurrence and intensity vary with solar flux, longitude sector, season, and magnetic activity. ESF occurrence and severity are also known to show a high degree of day-to-day variability. A large number of experimental and theoretical studies indicate that ESF is associated with an ionospheric plasma version of the Rayleigh-Taylor (RT) fluid instability [e.g., *Woodman and La Hoz*, 1976; *Sultan*, 1996]. More recent studies suggest that ESF could be a product of an ionospheric collisional shear (CS) instability [*Hysell and Kudeki*, 2004] or a combination of both RT and CS processes [*Aveiro and Hysell*, 2010]. We currently seek a better understanding of the processes leading to ESF, the sources of variability and ways to forecast its development. A better understanding of ESF is also motivated by its impact on the propagation of radio waves used for communication, navigation, and remote sensing [*Kintner et al.*, 2007].

The deployment of AMISR systems at high latitudes has allowed a number of advances in ionospheric studies in the auroral region [e.g., *Nishimura et al.*, 2010; *Lyons et al.*, 2010; *Akbari et al.*, 2013; *Bahcivan et al.*, 2014]. It is expected that such systems can also greatly help advance our understanding of different ionospheric processes at low latitude and midlatitude. The capability of steering the beam from pulse to pulse has been sought at Jicamarca for many years. The AMISR-14 provides this new capability at Jicamarca, which enables studies of the variability of scattering structures in the magnetic equatorial plane. Electronic beam steering is used at other radar sites [e.g., *Fukao et al.*, 2004], but the measurements are made off the magnetic equator and at conventional VHF frequencies. AMISR is capable of measuring irregularities with scale sizes that are about 1 order of magnitude smaller than those probed by VHF systems. With the proper number of AMISR panels, one could envision, for instance, incoherent scatter radar measurements of thermospheric wind profiles and gravity wave parameters. Nevertheless, with the current number of panels, we demonstrate that the system is sensitive enough to detect ESF ionospheric irregularities. Its frequency of operation (430–450 MHz) probes irregularities with scale sizes that are approximately 10 times smaller than those observed by the Jicamarca radar (0.34 m versus 3 m). We also demonstrate that the system can "image" scattering structures in the magnetic equatorial plane over a field-of-view (~40°) that is much wider than possible with the 50 MHz Jicamarca system.

2. Experiment Description

2.1. AMISR-14

The AMISR-14 panels are arranged in a 2 × 7 configuration with two rows of seven panels each aligned in the north-south direction. This antenna array configuration produces an antenna beam with a one-way half-power beam width (HPBW) of approximately 2° in the North-South direction and ~8° in the East-West direction. This configuration was chosen to maximize the sensitivity of the coherent backscatter radar observations.

Ionospheric *F* region observations were made at a frequency of 445 MHz. Therefore, we observed Bragg backscattering from irregularities with scale sizes of about 0.34 m. Soundings were made using 28 bit coded pulses. The baud length was 10 μs, and the interpulse period was 4 ms. The electronic beam steering capability of AMISR-14 allowed us to make observations at different pointing directions. For this first experiment,

Table 1. AMISR-14 and JULIA ESF Experiment Parameters

Parameter	AMISR-14 ESF Experiment	JULIA ESF Experiment
Frequency	445 MHz	50 MHz
Bragg wavelength	0.34 m	3 m
Panel configuration	7 (NS) × 2 (EW)	Not applicable
Peak power	224 kW	8 kW
Interpulse period (IPP)	4 ms	6.25 ms
Code length	28 bauds	Uncoded
Baud length	10 μs	25 μs
Antenna aperture	98 m^2	~32,000 m^2
Antenna HPBW (NS/EW)	2°/8°	1°/1°
Coherent integration	No	No
Incoherent integration	1280	240
Steering	Pulse-to-pulse ±25–35°	Not applicable

seven pointing directions were selected. One hundred twenty-eight pulses were transmitted in each look direction before switching positions. Five of the pointing directions were in the magnetic east-west plane and, therefore, provided soundings where the radar pointed perpendicular to the magnetic field. The remaining two beams were pointed 4.8° off zenith in the south and north directions. In these two directions, we made *F* region soundings with beams that were not pointed perpendicular to the magnetic field.

Detection of *F* region irregularities using this mode were attempted on four consecutive days: 19–22 August 2014. The average solar flux index ($F_{10.7}$) for the period was 128 sfu (1 sfu = 10–22 W m^{-2} Hz^{-1}), a period of low-to-moderate solar activity. The magnetic *Kp* index remained below 3 for the period of the observations except on 19 August, when *Kp* reached 4– and 5+ in the 19:00–21:00 UT and 21:00–24:00 UT 3 h windows, respectively.

Table 1 summarizes the main characteristics of the AMISR-14 system and lists the main parameters of the mode used for observations of ESF. See *Heinselman and Nicolls* [2008] for additional details about the AMISR system. Figure 1 describes the pointing positions used in these observations.

2.2. JULIA

Observations of *E* and *F* region equatorial field-aligned irregularities are made, regularly, at the JRO using the Jicamarca Unattended Long-term studies of the Ionosphere and Atmosphere (JULIA) system [e.g., *Hysell and Burcham*, 1998]. JULIA is a 50 MHz coherent scatter radar system, which utilizes some of the antenna hardware of the Jicamarca incoherent scatter radar combined with low-power transmitters for routine,

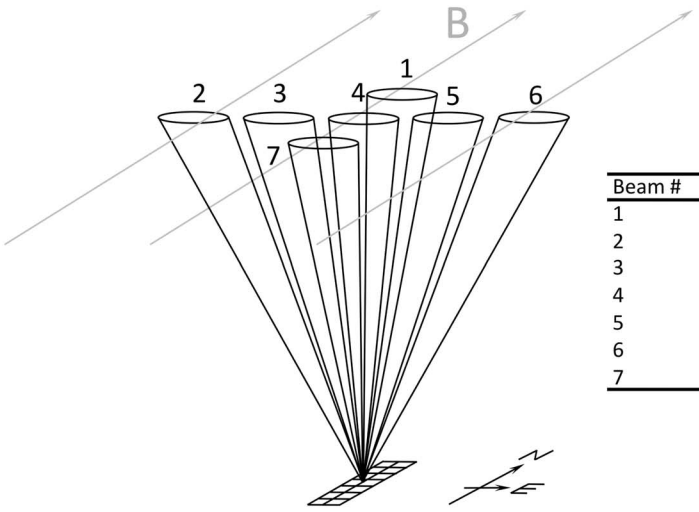

Beam #	Az	Elev
1	0°	85.2°
2	-90°	69.2°
3	-90°	80.4°
4	0°	90.0°
5	90°	80.4°
6	90°	69.2°
7	180°	85.2°

Figure 1. Pointing directions used in the *F* region experiments.

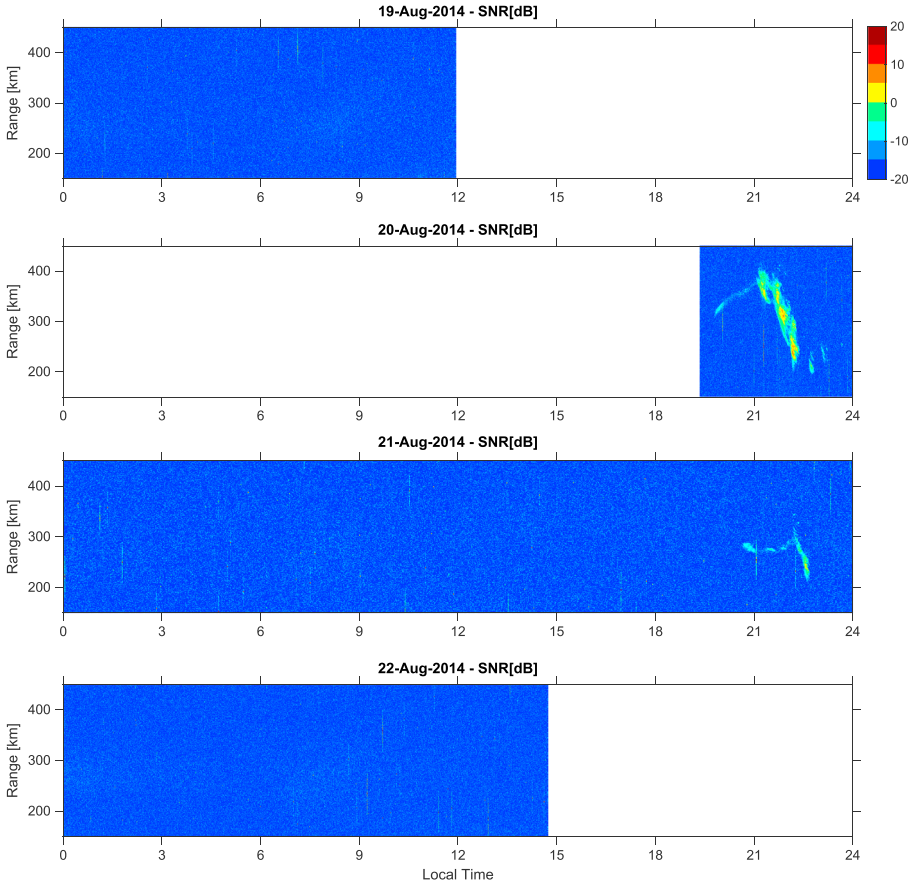

Figure 2. Range-Time-Intensity (RTI) maps of the *F* region measurements (vertical beam) made during this observation campaign.

uninterrupted observations. JULIA observations were made using two different modes: JULIA EW-ESF and JULIA imaging. The JULIA EW-ESF mode uses two beams in the EW plane to observe the occurrence of ESF echoes and determine the mean zonal and vertical drift of irregularities causing echoes. The JULIA imaging mode uses multiple receiving antennas to compute in-beam interferometric images of scattering structures. For this study, observations of the JULIA EW-ESF mode are used for comparison with AMISR-14 measurements. JULIA EW-ESF mode uses uncoded, 3.75 km long pulses with an IPP of 937.5 km. The highest height sampled with this mode is 930 km.

3. Results and Discussion

3.1. AMISR-14 Detection of *F* Region Echoes

Figure 2 shows the Range-Time-Intensity (RTI) maps created using the measurements made by the AMISR vertical beam during the observation campaign. The RTI maps show that observations were available for periods at night (premidnight and postmidnight) and, for some days, during daytime. Inspection of the RTI maps shows no *F* region echoes during daytime and postmidnight hours.

F region echoes are observed, predominantly, during nighttime, and only a few rare cases of daytime *F* region echoes were reported by the Jicamarca 50 MHz radar and elsewhere [*Chau and Woodman*, 2001; *Shume et al.*, 2013]. Therefore, it is not surprising that daytime UHF *F* region echoes were not detected. Postmidnight echoes were also not detected in the AMISR-14 observations. Postmidnight *F* region irregularities have been found to be associated with geomagnetic disturbances [e.g., *Hysell and Burcham*, 2002]. Unfortunately, observations were not available in the premidnight and postmidnight hours of 19/20 August after *Kp* reached 5^+. JULIA, however, was operating and did not detect any echoes during that time.

Our observations show that bottom-type and bottomside echoes were detected by AMISR-14 in the evenings of 20 and 21 August. An expanded view of the echoes observed on these days is given in Figure 3, and

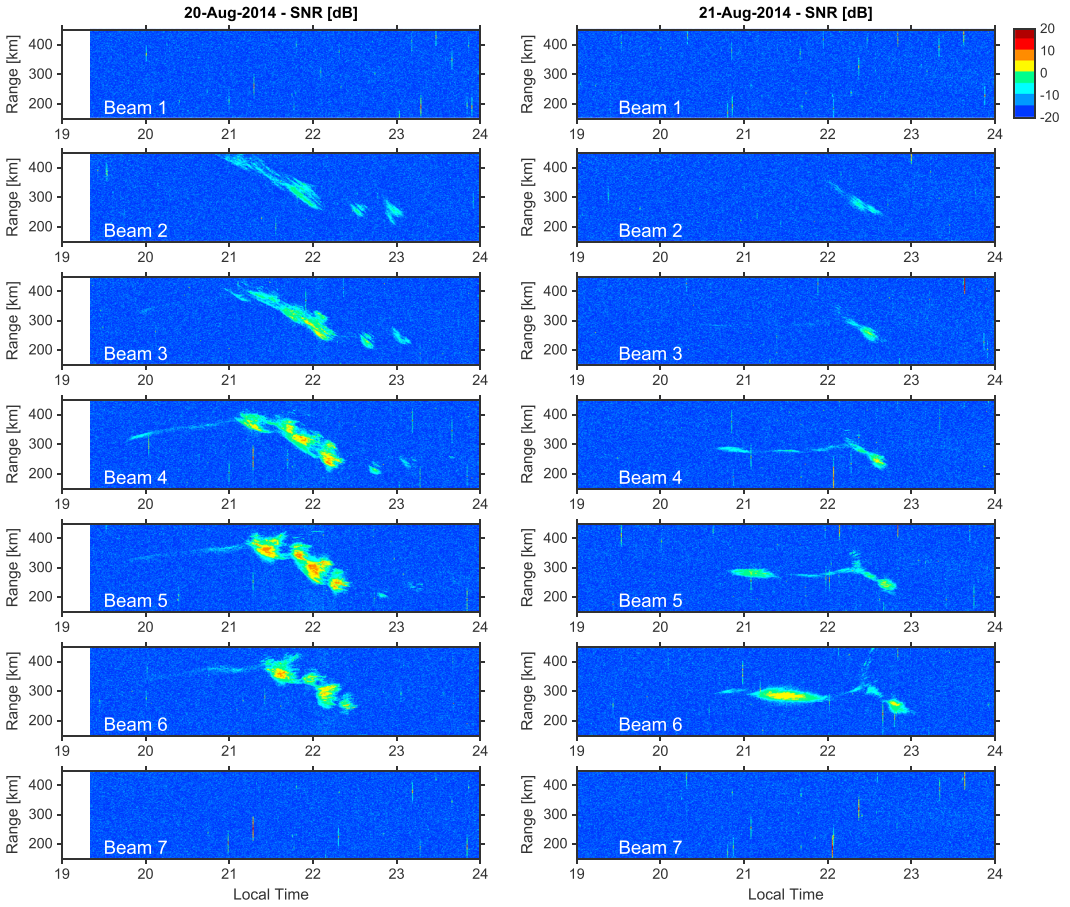

Figure 3. (left) The Range-Time-Intensity (RTI) maps of the *F* region observations made by each of the seven beams used by the AMISR-14 experiment on 19–22 August 2014. (right) The RTI maps for 21 August 2014. The beam number (see Figure 1) is indicated in each panel.

will be discussed in the following subsection. Bottom-type layers are identified, according to their RTI signatures. They are formed by vertically narrow, unstructured regions of relatively weak echoes [*Woodman and La Hoz*, 1976; *Hysell and Burcham*, 1998]. Bottomside echoing regions are also described as vertically undeveloped scattering regions. They are, however, more developed, structured, and cause stronger echoes than bottom-type irregularities [*Woodman and La Hoz*, 1976; *Hysell and Burcham*, 1998]. Bottomside echoes as strong as 10 dB above the noise level were detected in our observations.

3.2. Multibeam Observations

Figures 3 (left) and 3 (right) show more details of the observations made on 20 and 21 August, respectively. They show the RTI maps for each of the seven pointing directions (beams) used in the experiments. The beam number is indicated in each panel, and the beam directions are described in Figure 1.

First of all, the multibeam observations confirm the occurrence of submeter irregularities with off-vertical wave vectors. Noticeably, the observations show the detection of stronger bottom-type echoes by the vertical beam and by beams pointed to the east compared to echoes detected by the beams pointed to the west. Single-beam RTI maps would suggest that bottom-type layers are caused by a continuum of beam-filling irregularities. The multibeam observations, however, show significant variability in the occurrence of bottom-type irregularities over scales of several tens of kilometers in the zonal direction. We point out that observations made by the ALTAIR (Advanced Research Project Agency (ARPA) Long Range Tracking and Instrumentation Radar) also indicate such variability in the occurrence of bottom-type irregularities [e.g., *Hysell et al.*, 2006]. The long duration of ALTAIR mechanical scans (10–15 min), however, does not allow to distinguish spatial and temporal variations. The east-west variations in the occurrence and intensity of bottom-type echoes can be caused by spatial variations in the stability conditions and irregularity growth and, to a lesser degree, by

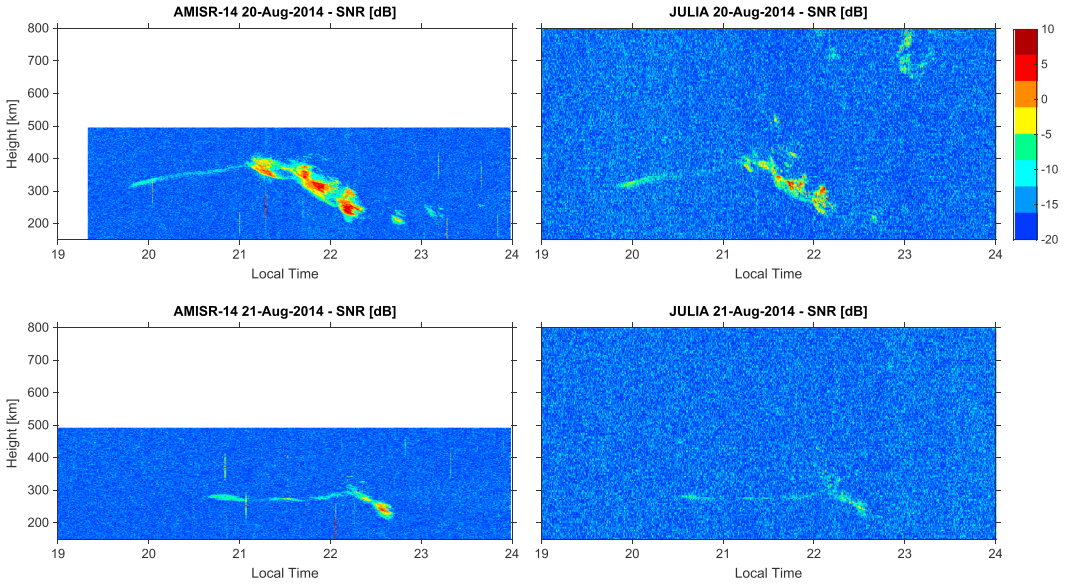

Figure 4. (left) The RTI maps for the AMISR-14 observations made on 20 and 21 August 2014. (right) The RTI maps for the JULIA observations. Both RTI maps use the same color scale.

differences in the aspect angle of the beams. We point out that large widths of the AMISR beams would minimize the aspect angle effect.

The observations also show a high degree of variability in the morphology of bottomside echoes from beam to beam. This variability is caused by zonal variations in the stability conditions leading to irregularities and by their highly dynamic behavior as they evolve and drift across the radar beams. Note that *F* region echoes were not detected by the beams pointed to the south and north of the radar site (beams 1 and 7). The lack of echoes is a result of the high degree of aspect sensitivity of ESF echoes [e.g., *Farley and Hysell*, 1996].

The RTI maps show that bottomside irregularities are observed by the westernmost beam first. Bottomside echoes are detected at later times by the other beams suggesting that irregularities drift in the eastward direction across the field of view of the radar. On 20 August, the first bottomside echoes are observed around 21:00 LT on beam 3. On beam 6, however, bottomside echoes only start to be observed around 21:30 LT. Considering that the beams are spaced by approximately 30° and the mean height of the irregularities is 350 km, the zonal velocity of the irregularities is estimated to be about 112 m/s toward the east. The magnitude and direction of the inferred irregularity velocity are comparable to the expectation of the mean *F* region zonal velocity [e.g., *Fejer et al.*, 2005].

Finally, on 21 August only weak bottom-type echoes are detected by the vertical beam between 20:00 and 21:00 LT. Relatively strong bottomside echoes, however, were detected by beam 6 (Az: 90° El: 69.2°). The steering capability can capture events that would be missed by a single beam radar. In fact, close inspection of the easternmost beam (beam 6 in Figure 3) shows a faint, narrow channel of echoes around 22:30 LT reaching the topside. The narrow channel of echoes is the signature of a radar plume that developed to the east of the radar site and that would have been missed by a single, vertical beam radar.

3.3. Meter and Submeter Irregularities

Figure 4 shows, side by side, the RTI maps of the observations made by JULIA and by the AMISR-14 vertical beam. The JULIA setup allowed measurements to much higher altitudes than the AMISR system. A comparison between the two RTIs at heights where both systems made observations shows that most features observed by JULIA are also observed by AMISR-14.

High-altitude echoes were observed by JULIA after 22:00 LT on 20 August at heights not sampled by AMISR. The AMISR RTI, however, does not show signatures of range-aliased high-altitude echoes. The lack of UHF echoes could indicate that the high-altitude structures were localized scatterers, which would not fill the wide beam of the AMISR system. The localized structure would produce UHF echoes that were not strong enough to be detected by AMISR. Additionally, the spectrum of ESF irregularities in the meter and submeter scale-size

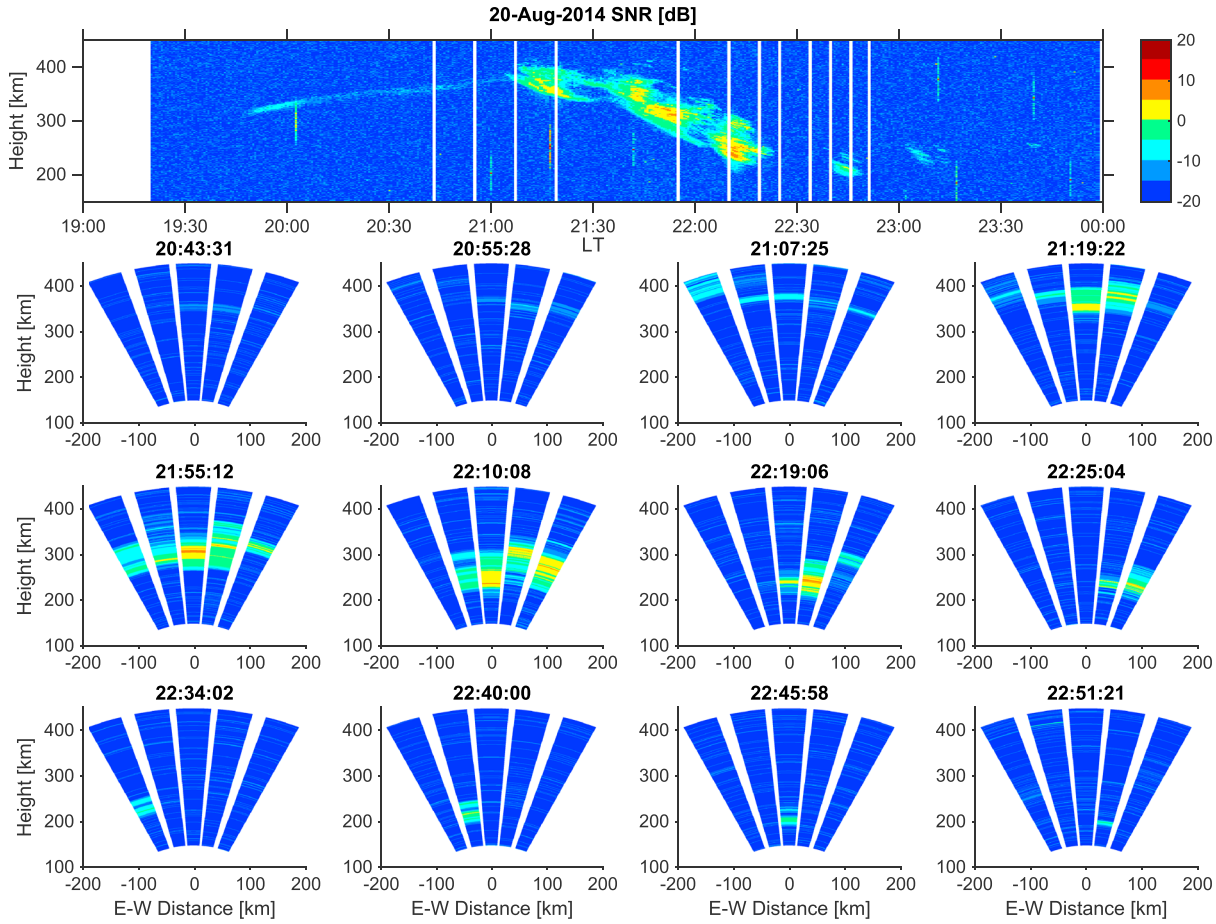

Figure 5. (top) The RTI map of the echoes observed by the AMISR-14 (vertical beam) on 20 August 2014. (second, third, and bottom rows) The RTI map showing "images" of the scattering structures created using the observations made by the five beams available for the ESF experiment.

ranges could be to be very steep [e.g., *Singh and Szuszczewicz*, 1984]. Therefore, the amplitude of submeter waves could be much smaller than the amplitude of meter-scale waves. This would contribute to a reduction in the scatter cross section at UHF and in the intensity of the echoes.

The interferometric in-beam imaging technique, one of the capabilities available at Jicamarca, will be used in the future to test this hypothesis and the response of AMISR-14 to different types of scattering structures. In-beam images have already shown that topside ESF echoes can be caused by very narrow (a few kilometers in the zonal direction) scattering regions [e.g., *Rodrigues et al.*, 2008].

3.4. East-West Dynamics

Figure 5 shows the first results of using the AMISR-14 electronic steering capability to construct two-dimensional "images" of the scattering structures causing radar echoes. A sequence of images can be used to create an animation of the dynamics of the scattering structures within the field of view of the radar.

Figure 5 (top) shows the RTI map of the observations made by the vertical beam on 20 August. Each of the panels below the RTI map shows a fan plot constructed with the five beams used for coherent backscatter observations. The fan plots show the echo intensity, for each beam, as a function of range, in the magnetic east-west plane. The angular width of each beam is approximately 8°, dictated by the HPBW of the antenna in the east-west plane. Vertical white lines in the RTI maps indicate the time for each fan plot. The time is also indicated on the top of each panel.

Figure 5 (second row) show the images created during the transition from bottom-type to bottomside echoes as shown by the RTI map. The images show that bottom-type irregularities are initially detected above and to the east of the radar site. No clear indication of zonal motion of the bottom-type irregularities is observed.

Then, stronger echoes associated with bottomside irregularities appear to the west of the radar site, move to the east, and obscure signatures of bottom-type echoes.

Figure 5 (third row) shows observations made during the occurrence of bottomside irregularities. The images show that the bottomside *F* region is disturbed at submeter scale sizes over a zonal distance of 200 km or more. The sequence of images also show that the irregularity layer is not tilted as the RTI would suggest. Instead, the tilt of the layer seen in the RTI map is caused by the downward motion of the irregularity layer. Finally, the sequence also shows that the scattering structure moves in the eastward direction.

Figure 5 (bottom row) highlights the potential of the AMISR-14 system to track scattering structures. It shows the passage of a small, isolated scattering region that drifts across the field of view of the radar. The scattering structure also descends in altitude and decays as it drifts toward the east. No echoes were observed by the time the scattering structure would have reached the easternmost beam. Considering that it took about 17 min for the structure, at about 200 km altitude, to move from the first beam to the fourth (angular separation of about ∼30°), one can estimate an average zonal velocity of 113 m/s in the eastward direction.

4. Conclusions

In the past, a seven-panel AMISR prototype system was deployed at the Jicamarca Radio Observatory (JRO). Measurements, however, showed that the sensitivity of the seven-panel system was not adequate for equatorial spread *F* (ESF) observations. In August 2014, a new 14-panel AMISR system was installed at Jicamarca. We tested the ability of the new system to detect UHF ESF echoes. We were able to successfully detect UHF echoes produced by bottom-type and bottomside ESF irregularities.

The AMISR-14 observations were made in conjunction with measurements from the VHF JULIA system. The strongest UHF echoes reached ∼10 dB while JULIA observations showed events producing relative weak VHF echoes compared to fully developed ESF plumes seen at other times. Joint observations made by AMISR-14 and JULIA showed collocated submeter and meter bottomside *F* region irregularities. Observations from both systems showed similar RTI maps during bottom-type and bottomside events. High-altitude echoes observed by JULIA, however, were not detected by AMISR-14. Unfortunately, a fully developed topside layer (radar plume) was not adequately detected during our campaign of observations.

The electronic beam-steering capability of the AMISR-14 system was also tested and used to investigate the dynamics of ESF events in the magnetic equatorial plane. We were able to track the development, zonal drift, and decay of ESF irregularities with a field of view much wider than ever possible at Jicamarca (±20° from zenith). We found a significant variability in the occurrence and intensity of echoes, particularly of those associated with bottom-type irregularities, along the zonal direction. Our results indicate that the system has sensitivity enough to divide the soundings into more than five beam positions. An increased number of beams will allow a better "imaging" of submeter ESF scattering structures. The wide field-of-view AMISR measurements is complementary to the high-resolution VHF in-beam interferometric imaging observations available at Jicamarca.

AMISR measures ionospheric irregularities with scale sizes that are about 10 times smaller than what is commonly observable at Jicamarca. This provides an opportunity for a better understanding of the variability of the electron density spectrum in the meter to submeter scale size range during ESF, equatorial electrojet and 150 km echo events.

Finally, AMISR-14 adds the capability of tracking field-aligned irregularities, while the Jicamarca incoherent scatter radar can be used to obtain information about the background ionospheric parameters.

Acknowledgments

Work at UT Dallas was supported by AFOSR (FA9550-13-1-0095) and NSF (AGS-1303658). Work at SRI International was supported by NSF Cooperative agreement AGS-1133009. Work at Anna G. Mendez University System was supported by NSF (AGS-1039593). C.M. acknowledges NSF support (IIA-1139862), which allowed student travel to Jicamarca. JULIA measurements used in this study were made available by the Jicamarca Radio Observatory, which is a facility of the Instituto Geofisico del Peru operated with support from the NSF AGS-0905448 through Cornell University. JULIA measurements and contact information can be found at http://jro.igp.gob.pe. Information about the AMISR-14 measurements presented in this study can be obtained by contacting Fabiano Rodrigues (fabiano@utdallas.edu).

The Editor thanks Robert Pfaff and an anonymous reviewer for their assistance in evaluating this paper.

References

Abdu, M. A., R. T. de Medeiros, J. H. A. Sobral, and J. A. Bittencourt (1983), Spread F plasma bubble vertical rise velocities determined from spaced ionosonde observations, *J. Geophys. Res.*, *88*(A11), 9197–9204, doi:10.1029/JA088iA11p09197.

Akbari, H., J. L. Semeter, M. J. Nicolls, M. Broughton, and J. W. LaBelle (2013), On the localization of auroral Langmuir turbulence in thin layers, *J. Geophys. Res. Space Physics*, *118*, 3576–3583, doi:10.1002/jgra.50314.

Aveiro, H. C., and D. L. Hysell (2010), Three-dimensional numerical simulation of equatorial f region plasma irregularities with bottomside shear flow, *J. Geophys. Res.*, *115*, A11321, doi:10.1029/2010JA015602.

Bahcivan, H., J. W. Cutler, J. C. Springmann, R. Doe, and M. J. Nicolls (2014), Magnetic aspect sensitivity of high-latitude E region irregularities measured by the RAX cubesat, *J. Geophys. Res. Space Physics*, *119*, 1233–1249, doi:10.1002/2013JA019547.

Chau, J. L., and R. F. Woodman (2001), Interferometric and dual beam observations of daytime spread-*F*-like irregularities over Jicamarca, *Geophys. Res. Lett.*, *28*(18), 3581–3584, doi:10.1029/2001GL013404.

Dougherty, J. P., and D. T. Farley (1960), A theory of incoherent scattering of radio waves by a plasma, *Proc. R. Soc. London, Ser. A*, *259*(1296), 79–99, doi:10.1098/rspa.1960.0212.
Farley, D. T., and D. L. Hysell (1996), Radar measurements of very small aspect angles in the equatorial ionosphere, *J. Geophys. Res.*, *101*(A3), 5177–5184, doi:10.1029/95JA02640.
Fejer, B. G., J. R. Souza, A. S. Santos, and A. E. Costa Pereira (2005), Climatology of *F* region zonal plasma drifts over Jicamarca, *J. Geophys. Res.*, *110*, A12310, doi:10.1029/2005JA011324.
Fukao, S., Y. Ozawa, T. Yokoyama, M. Yamamoto, and R. T. Tsunoda (2004), First observations of the spatial structure of *F* region 3-m-scale field-aligned irregularities with the equatorial atmosphere radar in Indonesia, *J. Geophys. Res.*, *109*, A02304, doi:10.1029/2003JA010096.
Heinselman, C. J., and M. J. Nicolls (2008), A Bayesian approach to electric field and E-region neutral wind estimation with the poker flat advanced modular incoherent scatter radar, *Radio Sci.*, *43*, RS5013, doi:10.1029/2007RS003805.
Huang, C.-S., M. C. Kelley, and D. L. Hysell (1993), Nonlinear Rayleigh-Taylor instabilities, atmospheric gravity waves and equatorial spread *F*, *J. Geophys. Res.*, *98*(A9), 15,631–15,642, doi:10.1029/93JA00762.
Huba, J. D., G. Joyce, J. Krall, C. L. Siefring, and P. A. Bernhardt (2010), Self-consistent modeling of equatorial dawn density depletions with SAMI3, *Geophys. Res. Lett.*, *37*, L03104, doi:10.1029/2009GL041492.
Hysell, D., and J. Burcham (2002), "Long term studies of equatorial spread-F using the Julia radar at Jicamarca", *J. Atmos. Sol. Terr. Phys.*, *64*(12–14), 1531–1543, doi:10.1016/S1364-6826(02)00091-3, equatorial Aeronomy.
Hysell, D. L., and J. D. Burcham (1998), Julia radar studies of equatorial spread *F*, *J. Geophys. Res.*, *103*(A12), 29,155–29,167, doi:10.1029/98JA02655.
Hysell, D. L., and E. Kudeki (2004), Collisional shear instability in the equatorial *F* region ionosphere, *J. Geophys. Res.*, *109*, A11301, doi:10.1029/2004JA010636.
Hysell, D. L., M. F. Larsen, C. M. Swenson, A. Barjatya, T. F. Wheeler, T. W. Bullett, M. F. Sarango, R. F. Woodman, J. L. Chau, and D. Sponseller (2006), Rocket and radar investigation of background electrodynamics and bottom-type scattering layers at the onset of equatorial spread F, *Ann. Geophys.*, *24*, 1387–1400.
Hysell, D. L., J. Drexler, E. B. Shume, J. L. Chau, D. E. Scipion, M. Vlasov, R. Cuevas, and C. Heinselman (2007), Combined radar observations of equatorial electrojet irregularities at Jicamarca, *Ann. Geophys.*, *25*(2), 457–473, doi:10.5194/angeo-25-457-2007.
Kagan, L. M., R. S. Kissack, M. C. Kelley, and R. Cuevas (2008), Unexpected rapid decrease in phase velocity of submeter Farley-Buneman waves with altitude, *Geophys. Res. Lett.*, *35*, L03106, doi:10.1029/2007GL032459.
Kelley, M. C., R. A. Cuevas, and D. L. Hysell (2008), Radar scatter from equatorial electrojet waves: An explanation for the constancy of the type I Doppler shift with zenith angle, *Geophys. Res. Lett.*, *35*, L04106, doi:10.1029/2007GL032848.
Kintner, P. M., B. M. Ldevina, and E. R. de Paula (2007), GPS and ionospheric scintillations, *Space Weather*, *5*, S09003, doi:10.1029/2006SW000260.
LaBelle, J., J.-M. Jahn, R. F. Pfaff, W. E. Swartz, J. H. A. Sobral, M. A. Abdu, P. Muralikrishna, and E. R. dePaula (1997), The Brazil/Guará equatorial spread F campaign: Results of the large scale measurements, *Geophys. Res. Lett.*, *24*(13), 1691–1694, doi:10.1029/97GL00818.
Lyons, L. R., Y. Nishimura, Y. Shi, S. Zou, H.-J. Kim, V. Angelopoulos, C. Heinselman, M. J. Nicolls, and K.-H. Fornacon (2010), Substorm triggering by new plasma intrusion: Incoherent-scatter radar observations, *J. Geophys. Res.*, *115*, A07223, doi:10.1029/2009JA015168.
Makela, J. J., and E. S. Miller (2008), Optical observations of the growth and day-to-day variability of equatorial plasma bubbles, *J. Geophys. Res.*, *113*, A03307, doi:10.1029/2007JA012661.
McClure, J. P., W. B. Hanson, and J. H. Hoffman (1977), Plasma bubbles and irregularities in the equatorial ionosphere, *J. Geophys. Res.*, *82*(19), 2650–2656, doi:10.1029/JA082i019p02650.
Nishimura, Y., et al. (2010), Preonset time sequence of auroral substorms: Coordinated observations by all-sky imagers, satellites, and radars, *J. Geophys. Res.*, *115*, A00I08, doi:10.1029/2010JA015832.
Retterer, J. M. (2010), Forecasting low-latitude radio scintillation with 3-D ionospheric plume models: 1. Plume model, *J. Geophys. Res.*, *115*, A03306, doi:10.1029/2008JA013839.
Rodrigues, F. S., D. L. Hysell, and E. R. de Paula (2008), Coherent backscatter radar imaging in Brazil: Large-scale waves in the bottomside F-region at the onset of equatorial spread F, *Ann. Geophys.*, *26*(11), 3355–3364, doi:10.5194/angeo-26-3355-2008.
Shume, E., F. Rodrigues, E. de Paula, I. Batista, M. Butala, and D. Galvan (2013), Day-time F region echoes observed by the São Luís radar, *J. Atmos. Sol. Terr. Phys.*, *103*, 48–55, doi:10.1016/j.jastp.2013.02.003.
Singh, M., and E. P. Szuszczewicz (1984), Composite equatorial spread *F* wave number spectra from medium to short wavelengths, *J. Geophys. Res.*, *89*(A4), 2313–2323, doi:10.1029/JA089iA04p02313.
Sultan, P. J. (1996), Linear theory and modeling of the Rayleigh-Taylor instability leading to the occurrence of equatorial spread F, *J. Geophys. Res.*, *101*(A12), 26,875–26,891, doi:10.1029/96JA00682.
Vlasov, M. N., M. C. Kelley, and D. L. Hysell (2007), Eddy turbulence parameters inferred from radar observations at Jicamarca, *Ann. Geophys.*, *25*, 475–481, doi:10.5194/angeo-25-475-2007.
Woodman, R. F. (2009), Spread F—An old equatorial aeronomy problem finally resolved?, *Ann. Geophys.*, *27*(5), 1915–1934, doi:10.5194/angeo-27-1915-2009.
Woodman, R. F., and C. La Hoz (1976), Radar observations of F region equatorial irregularities, *J. Geophys. Res.*, *81*(31), 5447–5466, doi:10.1029/JA081i031p05447.